RESEARCH PAPER

New insights into the 2017 Sefidsang earthquake by Coulomb stress change pattern and aftershock distributions: implication for active tectonics of NE Iran

Mahnaz Nedaei [1,2]* , Hasan Alizadeh [1]

[1] Department of Geology, Payame Noor University (PNU), 19395-4697 Tehran, Iran
[2] Board of directors of geological society of Iran

Abstract
The April 5th 2017 Mw 6.15 Sefidsang earthquake occurred east-northeast of the town of Fariman near the Cimmerian arc-related Fariman complex. The stress distribution was estimated by seismic parameters and Coulomb stress distribution in the source region. Inferred Coulomb stress field and general pattern of aftershocks distribution revealed that the Sefidsang earthquake occurred on a northeast-dipping listric fault with dextral reverse movement. Proximity of the Sefidsang sequence to Fariman complex proposes the reactivation of the pre-existing Cimmerian arc-related faults in the present-day stress field. The crustal-penetrating low-angle inverted faults coupled with Mesozoic mafic–ultramafic magmatism can shed light on the structural aspects of the region. The kinematics was also investigated by GPS velocity fields and morphotectonic features. The counterclockwise block rotation under the left-lateral regional shear between the Doruneh fault system and the North Kopeh Dagh fault system and NE-oriented coeval shortening led to the formation of rhombic structures. Cimmerian-related basement faults in NE Iran confined the expansion of rhombic cells and sense of block rotation. The results of this study improved our understanding about kinematics of active deformation in NE Iran and had important implications for seismic hazard assessment of the region and potential future failure area.

Keywords: Sefidsang Earthquake, Coulomb Stress, Spatial B-Value Variation, Cimmerian Arc-Related Fariman Complex, Rhombic Structure, Kopeh Dagh Mountains.

Introduction

As part of Alp-Himalayan fold-thrust orogenic belt, Iran reflects a long and complex tectonic history that results from the progressive collision and accretion of Gondwana-related blocks to the Eurasian margin in different times and tectonic regimes (Jackson & McKenzi, 1984). Various evidence like earthquakes in recent decades, semi-active volcanoes, rising beaches, rising salt domes, mud volcanoes, development of seismic faults, indicates geodynamic evolution of Iran is still in progress (Darvish Zadeh, 1991). Active continental deformations in Iran resulting from the northward motion of Arabia with respect to Eurasia, has a velocity of 22-25 mm/yr at longitude 57°E (McClusky et al., 2003; Vernant et al., 2004). The seismicity within Iran suggests that maximum deformation related to Arabia-Eurasia convergence is mainly concentrated in the Zagros, Alborz, Talesh and Kopeh Dagh mountain ranges, subduction beneath the central Caspian sea and the Makran, and on N-S right-lateral fault

---

* Corresponding author e-mail: mah_neda@yahoo.com

systems in East Iran representing different styles of deformation in various parts of this continental collision zone (Jackson, 1992; DeMets et al., 1994; Walker & Jackson, 2004). This deformation model is supported by the limited GPS data (Vernant et al., 2004; Masson et al., 2007). West of 57°E, the Zagros and the Alborz mountain ranges accommodate 6.5 ± 2 mm/yr and 8 ± 2 mm/yr respectively. The right-lateral displacement along the Main Recent Fault in the northern Zagros is ~3 ± 2 mm/yr, whereas ~8 ± 2 mm/yr is taken up in northwestern Iran. East of 57°E, most of the shortening is accommodated by the Makran subduction zone (19.5 ± 2 mm/yr), with the remainder (~6.5 ± 2 mm/yr) accommodated on various intracontinental mountain belts in East and NE Iran (Vernant et al., 2004).

On the continents, deformation is typically distributed over wide areas, and it is often unclear how fault systems accommodate regional strain (McKenzie & Jackson, 1986; England & Jackson, 1989; McCaffrey, 1991). Earthquakes as a result of an instability in faulting, are so pervasive that on many faults most slip occurs during them. Growth and development of faults take place by the cumulative action of earthquakes; therefore, the faults contain the history of past seismicity (Scholz, 1990). The seismicity is an extremely important resource to studies of both continental tectonics and seismic hazard assessment in deforming regions.

The Sefidsang earthquake occurred at 6:9 UTC on April 5th, 2017 Mw 6.15 at a depth about 11.5 km. Its epicenter was about 35.776 degrees of latitude and 60.436 degrees of longitude, ~30 km of Sefidsang and ~84 km southeast of Mashhad. The maximum acceleration of this earthquake recorded by Iranian Strong Motion Network was about 120 cm/s at Nasrabad Station, 38 km from the epicenter.

Focal mechanism solutions processed by some global seismological centers (Fig. 1) show reverse with minor strike slip mechanism of NW oriented fault. Based on the GSI field observations, the most destructive effects of earthquake were observed at Kuh-e Sefid and Derakht-e Bid villages near one of the Kashafrud fault segments known as the Chah-e Mazar reverse fault. InSAR displacement measurements computed by National Cartographic Center of Iran (NCCI) represent dip slip displacement about 15 centimeters and the fault rupture about 20 km (Naimi et al., 2017).

Although historical seismicity in the northeast of Iran is mostly associated with the Baghan, Quchan and Neyshabur faults (Tchalenko, 1975; Ambraseys & Melville, 1982; Berberian & Yeats, 1999; Berberian & Yeats, 2001)**,** the Sefidsang earthquake occurred in a region that has faced almost no historic or recent seismicity (Berberian & Yeats, 1999, Iranian Seismological Center [IRSC]) and has been characterized by low deformation rate with respect to the Eurasia (Masson et al., 2007). Even though seismic hazard information can be inferred from GPS velocities and related tectonic models, deformation of this type can be difficult to detect spatially by the low density and coarse distribution of GPS measurements (e.g., Masson et al., 2007; Mousavi et al., 2013). Therefore, detailed studies on the causative kinematics resulting in the Sefidsang earthquake gives an excellent opportunity to investigate both the pattern and kinematics of deformation in the current stress regime in NE Iran.

The Coulomb stress change is one of a number of models relating to the stress triggering in earthquakes (Hardebeck et al., 1998). Since the 1990s, the Coulomb stress change has been widely employed to probe the cause of triggering in several general types of studies: a) main shock-main shock triggering, b) main shock-aftershock triggering, and c) faults optimally oriented for failure. A large number of studies have investigated the Coulomb stress changes and earthquake interactions (e.g., King et al., 1994; Stein et al., 1994; Harris et al., 1995; Deng & Sykes, 1997; Hardebeck et al., 1998; Harris, 1998; Wang & Chen, 2001; Parsons, 2002; Wang et al., 2003; Lin & Stein, 2004; Steacy et al., 2005; Lin et al., 2011; Mitsakaki et al., 2012; Yadav et al., 2012; Catalli et al., 2013; Hainzl et al., 2014; Wang et al., 2014; Sarkarinejad & Ansari, 2014, 2015). There are recent works of Su et al. (2018) and Haji Aghajany et al. (2020) that applied the Coulomb stress change on the causative fault parameter determined by

InSAR technique to investigate the stress distribution after the Sefidsang earthquake triggering the aftershocks (the "b" category).

In this paper, Coulomb stress changes induced by regional stress (before the earthquake) are implemented to determine the optimally oriented nodal plane of the 2017 Sefidsang earthquake for failure. Our research lays in the "c" category of Coulomb stress studies mentioned above. We also investigated its interaction with the surrounding area using the correlation between the epicentral distribution of aftershocks and the increased Coulomb stress area promoting failure. Accordingly, the spatial changes of b-value were estimated for pre- and post-seismic data to disclose stress-accumulated and -released area, respectively. The thrust and strike-slip components of Kashafrud fault slip rates were estimated by resolving the GPS velocity of Mashhad station to realize the kinematics resulting in the Sefidsang mainshock. The kinematic evidence of active faulting in this area has also been discussed through the study of morphotectonic features. This multi-aspects study of the Sefidsang source area helps us to recognize the pattern of active tectonics. The results were discussed in the light of our knowledge of active tectonics in NE Iran and the previous work of Zanchetta et al. (2013) to construct a clearer image of geodynamics in a broader framework of the region. This research aims to improve our understanding about kinematics of NE Iran and has important implications for seismic hazard assessment of the region.
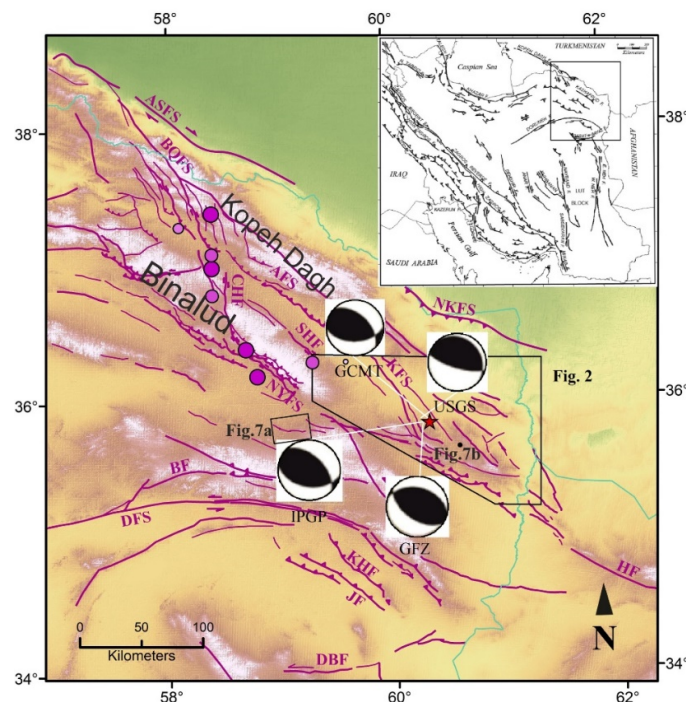

Figure 1. Inset: Active faults of Iran, modified from Berberian (1997). Main figure: Active faults, the epicenters of great historical earthquakes of NE Iran, the epicenter and focal mechanism solutions of the Sefidsang earthquake (2017.04.05) plotted over the SRTM 90m DEM. Focal mechanism solutions of the earthquake processed by international seismological centers show thrusting with minor strike slip component. The Sefidsang mainshock is shown as a red star. Violet circles present epicenters of historical earthquakes with magnitude above 6 from 1500 to 1965, modified after Tchalenko (1975), Ambraseys & Melville (1982). Reverse faults are shown with teeth on hanging-wall side and the sense of strike slip faults is marked by arrow. Faults without teeth or arrows: sense of slip unknown. Abbreviations for faults are ASFS: Ashkabad fault system, NKFS: North Kopeh Dagh fault system, AFS: Atrak fault system, BF: Bijvard fault, BQFS: Baghan-Quchan fault system, CHF: Chakaneh fault, DBF: Dasht-e-Bayaz fault, DFS: Doruneh fault system, HF: Herat fault, KFS: Kashafrud fault system, JF: Jangal fault, KHF: Khaf fault, SHF: Shandiz fault, NYFS: Neyshabur fault system

Tectonic framework

Geology

Due to the importance of the inherited geological structure in NE Iran dictating the pattern of present-day deformation, we briefly summarize the geological evolution of this region from published studies. The geological history of NE Iran involved a period of relative quiescence and stable shelf sedimentation during the Palaeozoic, followed by continental collision during the Mesozoic and Cenozoic, which continues today (Hollingsworth et al., 2010).

Between Permian and Triassic times, one of the major geodynamic events is the Late Triassic Cimmerian orogeny due to subduction of the Palaeotethys ocean under the Turan plate of Eurasia (Natal'in & Sengör, 2005). The Fariman and Darreh Anjir complexes placed along the southern active margin of the Eurasia illustrate arc-related magmatic activity since the Devonian up to the Middle Triassic (Natal'in & Sengör, 2005). A supra-subduction zone setting related to episodic extension in the upper plate of the northward Palaeotethys subduction represents the tectonic environment in which the Fariman and Darreh Anjir complexes were deposited (Zanchetta et al., 2013). Collision started in the Late Triassic and ended in the Late Jurassic, when the Central-and-East Iran microplate collided with Eurasia. The collision resulted in the closure of the Palaeotethys ocean along a suture zone recorded by several units cropping out east and south-east of Mashhad (NE Iran), along the southern part of the Kopeh Dagh (Berberian & King, 1981; Sengör, 1984; Alavi 1996). The emplacement of Torbat Jam and Mashhad granite (217 Ma; Karimpour et al., 2010) within deformed beds suggests ongoing collision-related deformation persisted also after the collisional phase. During the Cretaceous the Central-and-East Iran block became separated from Eurasia by a newly formed branch of the Neotethys ocean (Stöcklin, 1974). During the end of the Cretaceous and early Palaeocene, shortening along the northern margin of Neotethys resulted in the re-collision of the Central-and-East Iran microplate with Eurasia and emplacement the Sabzevar and Kuhe-Sorkh ophiolites across NE Iran, marking the onset of the Alpine-Himalayan Orogeny (Berberian 1981; Alavi 1996; Guest et al., 2006). Once Central-and-East Iran was resutured to Eurasia, subduction of Neotethys shifted to the southern margin of Central-and-East Iran (Hollingsworth et al., 2010).

Lyberis & Manby (1999) believed that the Mesozoic-Neogene Kopeh Dagh basin was deformed due to closure of the Neotethys ocean. The northward motion of Arabia formed the Kopeh Dagh mountains as a NW-SE trending active belt. The dominance of northwest-striking folds and NNW- to WNW-striking faults developed within Paleozoic to Pliocene rocks of the Kopeh Dagh (Shabanian et al., 2009). To the south of the Kopeh Dagh, the Binalud mountain range lies in parallel which is structurally and geologically the eastward continuation of Alborz mountains (Alavi, 1992). The boundary between the Binalud and the Kopeh Dagh mountains runs along the Atrak river valley where it closely parallels the Kashafrud reverse fault. East of Mashad, the Kashafrud fault system cuts across the Atrak-Kashafrud valley into the Binalud mountains and runs to the south of Fariman Complex (Fig. 2).

Active tectonics and seismicity

The present-day shortening across the SE Kopeh Dagh (~3 mm/yr; Masson et al., 2007) is distributed across the Kashafrud and North Kopeh Dagh thrust faults. The shortening accommodated by Kashafrud fault segments results in uplifting river deposits north of the fault by ~50 m (Hollingsworth, 2008). At present, Cenozoic tectonics affecting the southern portion of the Kopeh Dagh mountains sandwich the Fariman Complex between the Mashhad ophiolites to the NW and the Darreh Anjir Complex to the E, in a system of en échelon antiforms defining

the high mountain reliefs of the area (Zanchetta et al., 2013). These asymmetric (south-verging) folds, most of which are tectonically active indicate slip at depth on a north-dipping fault and accommodate part of regional shortening near the surface (Hollingsworth, 2008). The axial traces of these fault-bend-folds follow the same trend of the contractional structures deforming the post-Cimmerian successions (Zanchetta et al., 2013). Moreover, morphotectonic features including deflected and beheaded stream channels occurring along NW- and ENE-striking fault planes are visible in satellite images. These structural and morphotectonic features provide clear evidence for recent movements within the study area.

Almost all of the large earthquakes in NE Iran, with magnitudes ranging from 6.5 to 7.5, were directly assigned to the significant deep-seated fault systems such as the Baghan, Quchan and Neyshabur faults (Tchalenko, 1975; Ambraseys & Melville, 1982; Berberian & Yeats, 1999; Berberian & Yeats, 2001). However, the band of maximum destruction associated to these historical earthquakes appears to follow the trends of Quchan and Baghan faults connecting to the Neyshabur Fault system (Fig. 1). In contrast, other NW-striking faults such as Atrak and Kashafrud fault systems in eastern Kopeh Dagh, are characterized by low levels of seismicity (Shabanian et al., 2009). There are some reports of shaking in Mashhad city by moderate earthquakes in 1598, July 30th 1673 and 1687 which may be related to activity along the Shandiz dextral reverse fault (Ambraseys & Melville 1982). Obviously, the recent Sefidsang earthquake occurred in a seismicity gap, with no major destructive earthquakes (M>7.0) occurring over the last few centuries (Berberian & Yeats, 1999). It happened in the upper crust (depth 11.5 km) where the eastern segment of the Kashafrud reverse fault meets the Fariman complex (Fig. 2).

Material and Methods

The slip occurring on faults (referred as "source faults") during earthquakes, deforms the surrounding area and changes the stress field. A measure of this change is the Coulomb static stress (Mitsakaki et al., 2013; Meier et al., 2014).
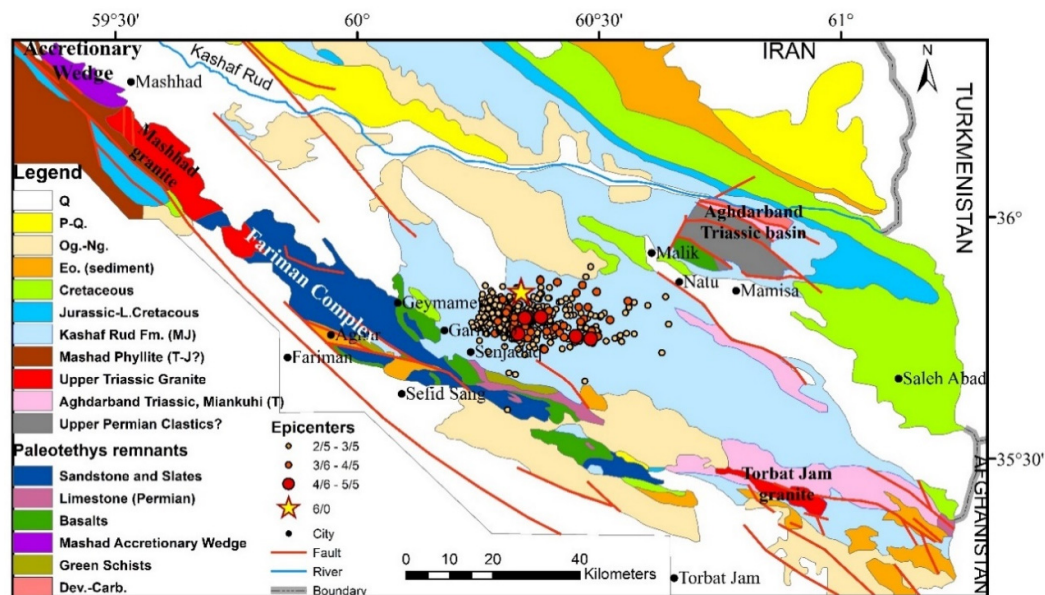

Figure 2. General geological map of the area presents uniform NW-striking fold and thrust faults developed in Pliocene to older Paleozoic rock units, modified after Ruttner (1991). See Figure 1 for the location. The Sefidsang earthquake sequence is shown by circles (the greater earthquakes, the greater circles). Yellow star marks the location of the Sefidsang mainshock

The Coulomb stress changes can be derived from strain created by displacement of a source fault. Therefore, the shear and normal components of the stress change can be resolved on an area or on specified "receiver" fault planes. Receiver faults are planes with a specified strike, dip, and rake, on which the stresses imparted by the source faults or tectonic regime. In other representation, the faults having optimal orientation with respect to the regional (also called "tectonic") stress or the stress imparted by the source fault, and the assumed friction coefficient are suitable for sliding and could be as a receiver fault. The Coulomb failure stress change, ΔCFS, is defined as (Das & Scholz, 1981; Stein *et al.,* 1992; Harris, 1998):

$$\Delta\sigma_f(\Delta CFS) = \Delta\tau_s + \mu'\Delta\sigma_{n'} \tag{1}$$

where $\Delta\tau_s$ is the change in shear stress on the receiver fault (set positive in the direction of fault slip), $\Delta\sigma_{n'}$ is the change in normal stress acting on the target fault (set positive for unclamping) and μ' is the effective coefficient of friction (Stein, 1999; Toda, 2008). The shear stress increase or decrease is dependent on the position, geometry, and slip of the source fault and on the position and geometry of the receiver fault, including its rake. The normal stress change is independent of the receiver fault rake. The parameter μ' is often called the apparent coefficient of friction and is intended to include the effects of pore pressure changes as well as the material properties of the fault zone (Harris, 1998). Fault friction μ' is often inferred to be 0.4-0.8 for faults with little cumulative slip, which tend to be rough, and 0-0.4 for faults with great cumulative slip, which tend to be smooth (Ma et al., 2005). This parameter is typically found to be around 0.4 for strike-slip faults or faults with unknown orientation (Parsons et al., 1999; Sumy et al., 2014).

The positive ΔCFS (the warm colored regions on Coulomb map) indicates that the plane of interest was brought closer to failure; the negative ΔCFS (the cool colored regions on Coulomb map) indicates that the plane of interest was moved away from failure. Both increased shear and unclamping of faults promote failure (Stein et al., 1997; Harris & Simpson, 1998; Parsons, 2005; Toda et al., 2008; Aron & Hardebeck, 2009). The Coulomb stress change depends on the geometry and slip of the earthquake, the geometry and sense of slip of the fault and the effective coefficient of friction (Stein et al., 1994).

There are two principal considerations of the Coulomb stress changes on receiver faults: stress changes on the specified receiver fault and stress changes on an optimally oriented receiver fault. The specified receiver faults rely on resolving stress changes on faults with known geometry (Ma et al., 2005; Hainzl et al., 2010). The optimally oriented receiver faults are determined by assuming that the earthquakes will be triggered only on those planes with maximum total Coulomb stress (King et al., 1994; Lin & Stein, 2004; Ishibe et al., 2011; Catalli & Chan, 2012).

The Gutenberg & Richter (1944) relation describes the number of earthquakes occurring in a given region as a function of their magnitude M as $log\ N = a - bM$; where N is the cumulative number of earthquakes with magnitude equal to or larger than M, *a* and *b* are real constants that may vary in space and time. The intercept ''*a*'' characterizes the general level of seismicity in a given area during the study period (i.e., the total number of earthquakes), while the slope ''*b*'' describes the relative size distribution of earthquakes. The parameter *b* can be estimated either by linear least squares regression or by maximum-likelihood using the equation (Aki, 1965; Ustu, 1965; Bender, 1983):

$$b = \frac{1}{\bar{M} - M_{min}} log\ e \tag{2}$$

where $\bar{M}$ denotes the mean magnitude and M_{min} the minimum magnitude of the given

sample. The determination of M_{min} relies on the magnitude distribution. Generally and practically, the minimum magnitude, M_{min}, is considered to be equal to the magnitude of completeness. The magnitude of completeness, M_C, is determined by plotting the cumulative number of events as a function of magnitude. These plots are then fitted with a straight line and M_C is the level at which the data fall below the line.

General "global" average value of the b parameter, obtained by mixing different crustal rock volumes and different tectonic regimes, is close to unity. The b-value is believed to depend on the stress regime and tectonic character of the region (Allen et al., 1965; Mogi, 1967; Hatzidimitriou et al., 1985; Tsapanos, 1990). Statistically significant changes of b-values have been extensively studied for various stress regimes such as a subducting slab (Wyss et al., 2001), along fault zones (Wiemer & Wyss, 1997) and in aftershock zones (Wiemer & Katsumata, 1999). Based on seismicity studies, Schorlemmer & Wiemer (2005) suggested that the b-value can be used as a «stressmeter». Regionally, changes in b-value are believed to be inversely related to changes in the stress level (Bufe, 1970; Gibowicz, 1973). Observations of locally changes in b-values compared to the global average value, also reflect the effective stress (Scholz, 1968). An increase of applied shear stress or effective stress results in decrease of b-value (Urbancic et al., 1992; Wyss, 1973). Low b-values have been correlated to areas of asperity, locked part of a fault where the nucleation of earthquakes is likely to happen (Schorlemmer et al., 2004, Tormann et al., 2012). High b-values have been correlated to the highest slip during large earthquakes (Görgün et al., 2009; Sobiesiak et al., 2007).

The state of stress

In this research, recorded data by the Iranian Seismological Center (IRSC, irsc.ut.ac.ir) and also collected by the International Seismological Centre (ISC) from 2006 (once the data has been completely recorded) to 2018 by M_N have been used. According to the focal mechanism solutions from the Global CMT and moment tensor solutions determined by the USGS, the mechanism of the Sefidsang earthquake is reverse with minor strike slip on northwest-southeast oriented nodal planes. The Wells & Coppersmith (BSSA, 1994) empirical magnitude-area relations were used to estimate appropriate rupture area. The characteristic of two nodal planes and the event are presented in Table 1.

The optimally oriented receiver fault is determined by assuming that the earthquake will be triggered only on plane with maximum total Coulomb stress and vice versa, the causative fault triggering the earthquake should have maximum Coulomb stress with respect to regional stress. Though in such a moderate earthquake that the causative fault of which is not exposed at the surface, theoretically, each nodal plane has the same possibility for failure, but following the rules of focal mechanism inversion (Carey-Gailhardis & Mercier 1987), one of them must be selected for each earthquake. Therefore, to specify the earthquake causative fault confidently, we should select the nodal plane on which imparted Coulomb stress is maximum. The best-fitting regional stress tensor compatible with the majority of ISC collected earthquake focal mechanisms over the period of years was defined by WinTensor program (Table 2).

The stress change calculations were performed using the software Coulomb 3.3 (Toda et al., 2011). For all the calculations of the Coulomb stress change, the shear modulus (G), 32×10^5 bar, Poisson ratio (v) 0.25, Young modulus (E) 8×10^5 bar and effective coefficient of friction (μ') 0.6 were used. The nodal plane resulting in the greatest consistency with the inferred Coulomb stress field (lying in red region on the Coulomb map), should be selected. However, the results shown in Figure 3a represents both nodal planes, more or less, were located in the positive ΔCFS area. It is also visible that the maximum Coulomb stress region is fully compatible with the uplifted area in the InSAR surface displacement measurements computed by the Iranian Space Agency, reflecting appropriate assumed parameters for Coulomb stress

change calculations (Fig. 3b). The calculated positive ΔCFS area is exactly placed where the Kashafrud fault bends in vicinity of Fariman complex.

The aftershocks preferentially occur in the calculated stress increase and less likely in the calculated stress decrease areas (Parsons et al., 2014). Therefore, the aftershocks tried to control which nodal plane has more matching with both high Coulomb stress and aftershocks distribution. The epicentral distribution of aftershocks by $M_N \geq 2$ and ≥ 3, mostly placed in the maximum (most positive) Coulomb stress area (Fig. 4), is more consistent with the first nodal plane in Table 1.

Due to the general pattern of aftershocks, it is obvious that the geometry of this nodal plane (namely Sefidsang earthquake causative fault) couldn't be planar and must be steepened at the upper part, in the form of listric faults.

Some factors such as, unknown stress concentration prior to the main shock, crustal heterogeneity and the existence of small faults with different orientations (Mitsakaki et al., 2013; Xie et al., 2014; Kozłowska et al., 2015) may play a role in perturbing the stress field and thus it is not surprising that all of the aftershocks have not been completely matched with regions of increased Coulomb stress.

The state of the stress distribution was also investigated by the b-value spatial change map. The b-value is a tool to monitor the state of stress along a fault zone and has a negative correlation with the differential stress.

Table 1. The geometry of the Sefidsang earthquake nodal planes taken from GCMT and ISC

Date	Time (UTC)	Lat (°N)	Lon (°E)	Depth (km)	Mw	Mechanism			Length (km)	Width (km)
						Strike (°)	Dip (°)	Rake (°)		
2017-04-05	6:9	35.776	60.436	11.5	6.15	316	20	120	13	8.18
						105	73	80		

Table 2. Principle stress direction

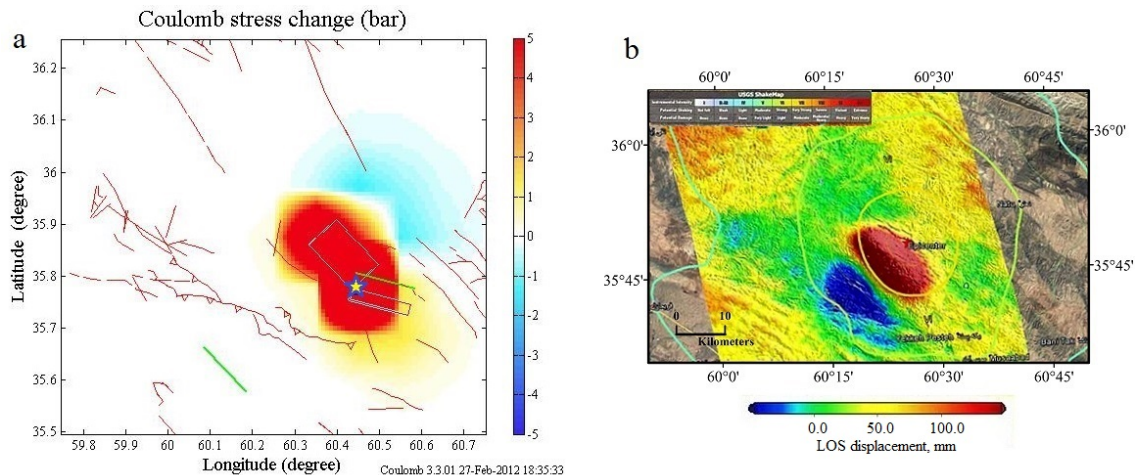|	σ_1	σ_2	σ_3
Trend	216	120	317
Plunge	8	35	54

Figure 3. a) Coulomb stress change for the Sefidsang earthquake nodal planes with respect to regional stresses. Red area represents the maximum Coulomb stress region. White rectangles show the hypothetical ruptures at focal depth based on Wells & Coppersmith relation and nodal planes geometry. Green lines represent the assumptive fault traces on the ground. The epicenter was shown by yellow star. b) The InSAR surface displacement model for Sefidsang earthquake adapted from ISA
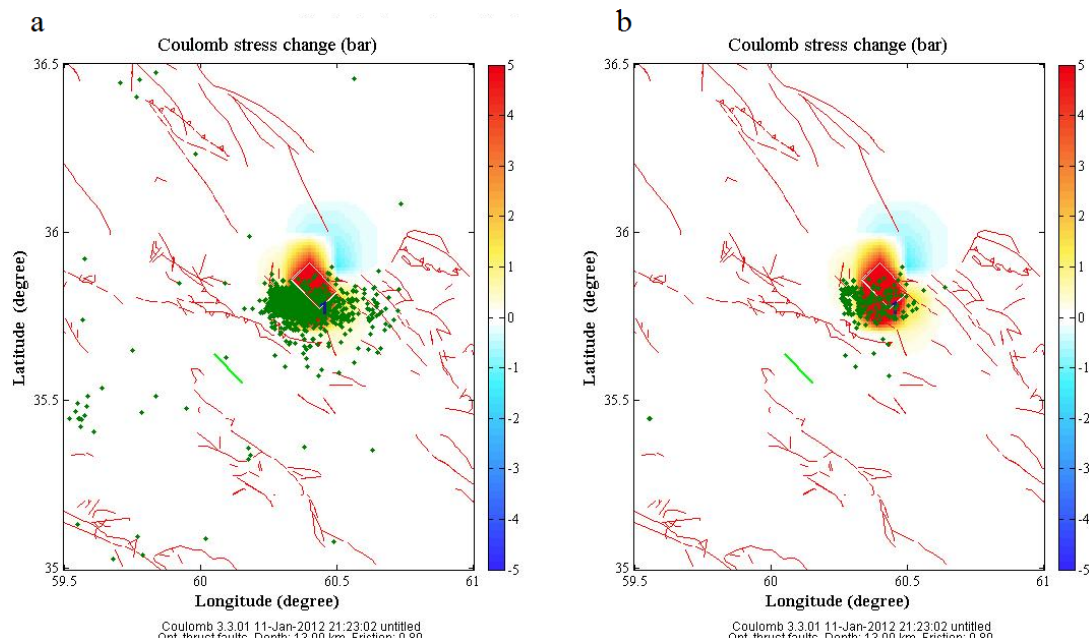
Figure 4. Distribution of aftershock events (green dots) in the maximum Coulomb stress area is more compatible with the first geometry of nodal planes in Table 1 (see figure 3a for more comparison). Limited epicentral distribution of aftershocks to the area before the assumptive fault trace on the ground (green line at the coulomb map) suggests a listric than a planar form of the causative fault. a) The magnitude of aftershocks is greater than 2. b) The magnitude of aftershocks is greater than 3. As it is shown, most of the aftershocks have well matched with maximum Coulomb stress area

To certify a homogeneous level of catalog completeness, the minimum magnitude of completeness (Mc) constraining the b-value map, should be estimated (Wiemer & Wyss, 2000) or could be specified by homogeneity assumption of catalogue (Schorlemmer et al., 2004). We estimated Mc of the IRSC catalog from 2006 to 2018 using the maximum curvature method by Zmap software to be 1.7 (Wiemer, 2001). It means that above this magnitude, the catalog is complete.

The spatial distribution of b-value was estimated by the maximum likelihood method using constant radius (R=50 Km, selected by considering the rate of seismicity of the area) for pre- and post-event datasets. The results obtained by Zmap software were represented in Figure 5. The spatial b-value change estimated from pre-event dataset represents low value around mainshock epicenter in correlation with increased applied shear stress or effective stress area (Urbancic et al., 1992; Wyss, 1973). In this regard, a comparison between the b-value map of pre-event dataset and the Coulomb stress changes displays good agreement between the region with low b-values and the positive Coulomb stress area.

However, the post-event dataset (from April 5th 2017 until the end of June 2018) contains a short period of time to set a detailed b-value map, but it shows high spatial b-value due to numerous seismic slips after the main shock at the same area having low b-value derived from pre-event dataset. The low b-value zone of pre-event and high b-value of post-event datasets, characterize stress accumulation and realization, respectively.

Active fault kinematics

By resolving the GPS velocity (Masson et al., 2007) of MSHN (Mashhad station) relative to Eurasia onto its respective thrust and strike-slip components, approximate slip rates may be estimated for Kashafrud fault segments. Since the strike of Kashafrud fault changes where it

crosses the Atrak valley, NE of Mashad, the velocity of MSHN (2.7±1.4 mm/yr) is slightly oblique to the Kopeh Dagh range front and a right-lateral component must also be accommodated across the fault system. Resolving this value onto thrust and strike-slip components indicates not exact but respective slip components across the SE Kopeh Dagh (Fig. 6). The junction area of two segments having relatively high thrust (~2.1 mm/yr) and right-lateral strike-slip (~2.2 mm/yr) rates is the location of Sefidsang earthquake sequence where the Kashafrud fault bends in vicinity of Fariman complex.

Deflected and beheaded stream channels occurring along fault planes and visible in satellite images, are the kinematic evidence of active faulting in the area (Fig. 7). These faults reveal sinistral and dextral reverse movements by affecting Quaternary deposits and provide clear evidence for recent movements.
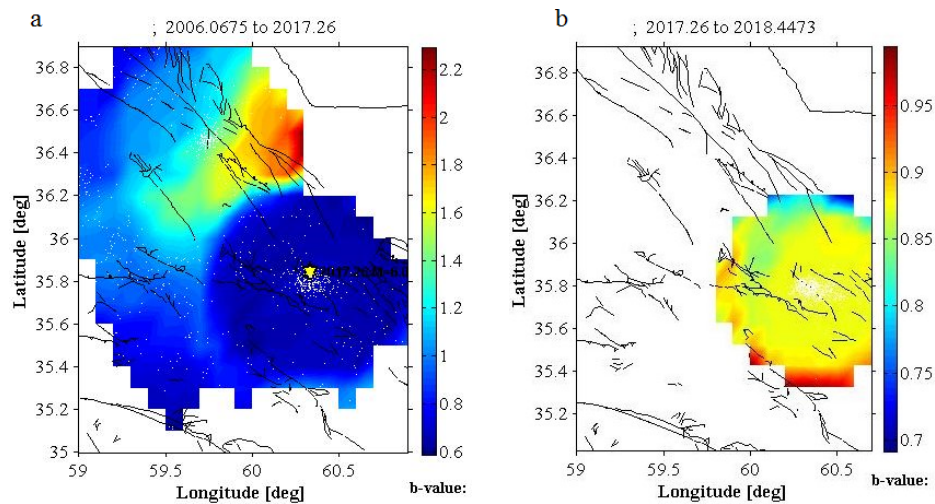

Figure 5. The calculated spatial distribution of b-value for pre- and post-Sefidsang event datasets. a) Dark blue area in the map shows low spatial b-value derived from pre-event dataset. The location of the Sefidsang mainshock was marked by yellow star. The extension of the area depends on the selected radius for calculation the b-value. b) Yellow area represents high b-value due to numerous seismic slips after the mainshock
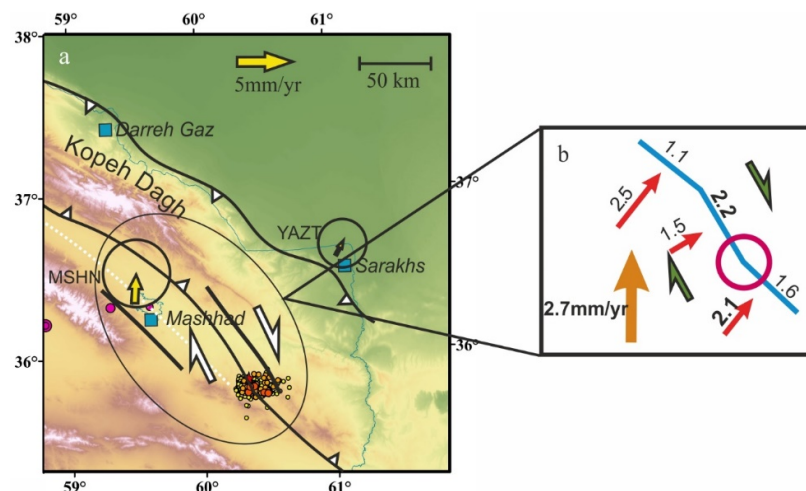

Figure 6. a) Simplified fault map (black lines) plotted over the SRTM 90m DEM of the Kopeh Dagh region. The Sefidsang earthquake sequence is shown by orange different size circles. Pink circles show historical earthquakes. Yellow arrows show GPS velocities, with respect to Eurasia from Masson et al. (2007). Blue squares show locations of towns and cities. White dotted line shows the Atrak-Kashafrud valley which divides the Kopeh Dagh from the East Alborz-Binalud. b) Velocity triangle constructions

using the motion of station MSHN to Eurasia, indicates different thrust and right-lateral strike-slip rates onto each segment of the Kashafrud fault across the SE Kopeh Dagh. The numbers represent the rates of thrust components shown by red arrows and strike-slip components set along the fault. The hollow pink circle at the junction of two segments is the location of Sefidsang earthquake sequence having relatively high thrust (~2.1 mm/yr) and right-lateral strike-slip (~2.2 mm/yr) rates.
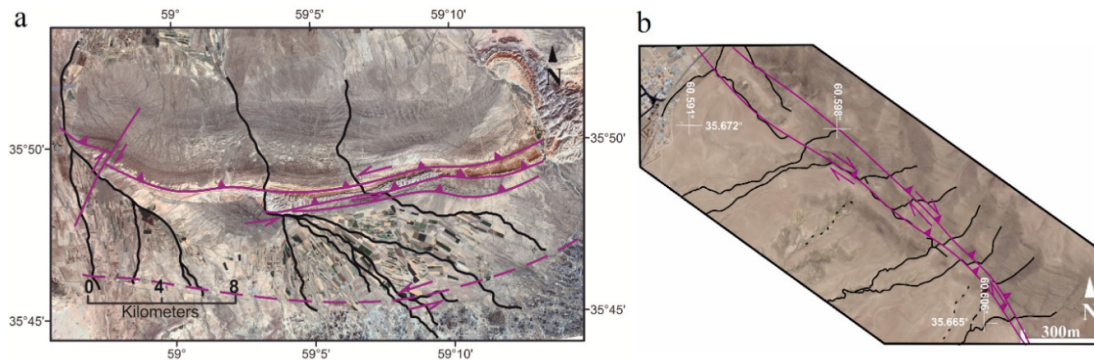

Figure 7. Google Earth image of stream channel systematic deflections and strike-slip offsets along active faults in the study area. See Figure 1 for the location. Black lines show active stream channels, dashed lines are abandoned streams, violet lines show the surface trace of active faults. a) Sinistral strike-slip offsets along ENE-striking reverse faults. b) Dextral strike-slip displacements along minor NW-striking reverse faults

Discussion

In order to characterize the regional active deformation, we need to understand the geometry and kinematics of the Sefidsang earthquake causative fault. In doing so, the inferred Coulomb stress change triggering the April 5th 2017 Mw 6.15 Sefidsang earthquake (pre-event stress) was calculated. Earthquakes are triggered on optimally orientated faults with respect to regional stress tensor having maximum Coulomb stress. Though, each of focal mechanism nodal planes could be theoretically the fault plane, but the one resulting in the greatest consistency with the inferred Coulomb stress field (lying on the positive ΔCFS region of the Coulomb map), on one hand, and the epicentral distribution of aftershocks, on the other hand, is the optimally oriented closer to failure and to be selected. The best-fitting regional stress tensor compatible with the majority of ISC collected earthquake focal mechanisms over the period of years was defined by WinTensor program (Table 2). Based on these assumptions, the Coulomb stress change was calculated with respect to regional stress and the status of ΔCFS distribution was investigated to identify which nodal plane has been more consistent with high Coulomb stress. Although Inferred Coulomb stress field by regional stress is consistent with both nodal planes, the epicentral distribution of aftershocks mostly placed in the maximum Coulomb stress area (Fig. 4) confirmed the nodal plane with 316º strike, 20º dip to the north and 120º rake geometry as the causative fault. From the general pattern of aftershocks distribution, it is also obvious that the geometry of the Sefidsang earthquake causative fault could not be planar and must be steepened at the upper part, in the form of listric faults.

  Based on a nonlinear inversion method composed of artificial neural network (ANN) and genetic algorithm (GA), Haji Aghajany et al. (2020) suggested the Sefidsang fault parameters as 210º for strike, 55º for dip and 154º for rake without any declaration of fault mechanism. The NE-striking fault plane obtained by the nonlinear inversion method is incompatible with their first suggestion from InSAR measurements and also NW-SE dominant trend of folds and faults in the region. Despite their inferred NE strike for the fault plane, they resolved the Coulomb model on a NW-striking fault plane to calculate the post seismic stress and strain. In another study of this earthquake, also based on InSAR measurements and modeling, Su et al. (2018)

proposed major dextral with minor reverse displacements (maximum 95 and 47 cm for strike-slip and dip-slip components, respectively), on a fault plane with 324° strike, 37.5° dip and 131.1° rake at a depth ~3.5 km. Their reported fault parameters are more compatible with a dominantly reverse kinematic than their proposed predominantly dextral one. In addition, based on the Wells & Coppersmith (1994) relations, a Mw 6.16 seismic event at a depth of ~3.5 km must have been accompanied by surface rupture but coseismic slip of the Sefidsang fault did not propagate to the ground. They calculated the Coulomb static stress change to examine the future seismic hazard in the Sefidsang source region.

The state of the stress distribution was also investigated by the b-value spatial change map. A Comparison of the b-value map estimated from pre-event dataset with the Coulomb stress changes displays a good agreement between the region with low b-values and the positive Coulomb stress area (Fig. 5).

Resolving NNE GPS velocity of station MSHN relative to Eurasia onto thrust and strike-slip components for each segment of the Kashafrud fault, indicates the junction area of two segments having relatively high slip rates is the location of Sefidsang earthquake sequence (Fig. 6). Although the NNW-SSE extent of calculated positive ΔCFS area and also the strike of fault bend have relatively high resolved slip rates, the aftershocks distribution is nearly east-west (Fig. 4a). Perturbing the stress field and therefore poor compatibility of aftershocks distribution with increased Coulomb stress regions, may be due to crustal heterogeneity and existence of different azimuthal oriented faults. If the stress tensor is insufficient to form a new fault, because of low frictional strength relative to necessary stress forming faults, pre-existing faults constituting weak planes may be reactivated (Scholz, 1990).

This reason from one side and proximity of the Sefidsang sequence to Fariman complex on the other side, debate reactivation of Cimmerian arc-related faults as planes of weakness in the crust in NE Iran. The Fariman complex were formed as a fault-controlled arc-related basin on the southernmost active margin of the Turan domain of Eurasia, under which the northward subduction of the Palaeotethys occurred. A supra-subduction zone setting characterized by several episodes of arc-splitting and basin opening, related to episodic extension in the upper plate, represents the tectonic environment in which the Fariman complex was deposited. During crustal-scale extension and isostatic compensation, low-angle extensional faults are formed with low initial dips sometimes penetrating in the lower crust and Moho is elevated and a metamorphic core complex is developed. By the Late Triassic, collisional phase constituting the final stage of the Cimmerian event made the crust contract. Under these circumstances, the crust contraction is easily done by reversal slip on pre-existing normal faults. Similarly, pre-existing faults will become reactivated if they have a favorable orientation of slip. This phenomenon, and the opposite (reverse faults being reactivated as normal faults) are commonly referred to as inversion. The tectonic contacts between Fariman units representing a previous low-angle normal faults correspond to a recent shear zone (Zanchetta et al., 2013). Therefore, it is very likely that the listric form of the northeast-dipping dextral reverse causative fault confirmed by the pattern of aftershocks distribution in Coulomb stress change map, is the inverted arc-related structures reactivated in recent tectonic regime. Figure 8 represents a kinematic model of fault planes reactivated during the Sefidsang earthquake sequence.

In this way, teleseismic tomographic results of Motaghi et al. (2012) have revealed an intra-crustal discontinuity beneath the Binalud (dashed line in tomographic cross section of Fig. 8) interpreted as the thickening of the crust beneath Binalud. Their results also show the lithosphere is thickened under the place that thickening of crust happened in similar way for the crust.
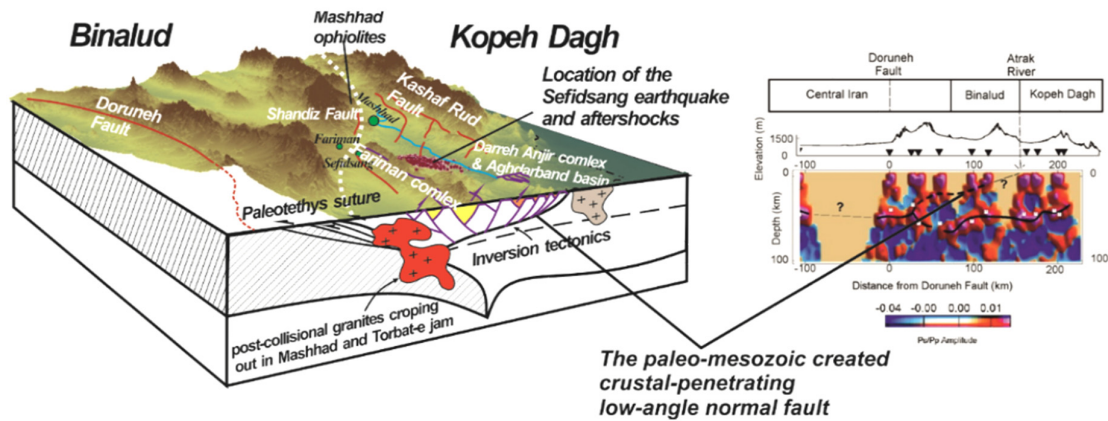
Figure 8. Conceptual model illustrating reactivated preexisting normal faults as reverse faults in current tectonic regime and 3D topographic relief of SRTM 90m DEM on it, viewed from S70°E. The Sefidsang earthquake sequence is shown by red circles on the top. Right picture shows seismic tomographic cross section computed by Motaghi et al. (2012) along the S44°W profile. The inferred position of the Moho by Motaghi et al. (2012) is marked by black lines. An intra-crustal discontinuity is seen beneath the Binalud (black dashed line). What is attributed as underthrusting of Turan Platform beneath Central Iran by them is thick-skin tectonics including crustal-penetrating low-angle faulting reactivated in current stress field coupled with mafic-ultramafic magmatism in the lower crust

Although geological evidences strongly confirm subduction of the north-directed Palaeotethys ocean, they suggested underthrusting of Turan Platform beneath Central Iran is responsible for this thickening. Now, the crustal discontinuity in tomographic results of Motaghi et al. (2012) can be explained by crustal-penetrating low-angle faults coupled with mafic-ultramafic magmatism in the lower crust representing thick-skin tectonics.

Morphotectonic features such as fault scarp lines, deflected and beheaded stream channels occurring along fault planes are the youngest kinematic evidences of active faulting in the area that affect Quaternary deposits by sinistral and dextral reverse movements (Fig. 7).

Interestingly, kinematics of fault planes reactivated during the Sefidsang earthquake sequence and other active faults of the region (i.e. Fig. 7) fall into larger kinematic framework that are compatible to a typical structural pattern namely the rhombic pattern. This structure implies similar dextral reverse kinematics for other NW-striking and sinistral reverse for ENE-striking faults distributed in the region, playing the role of linkage between distinct block-bounding fault systems of NE Iran. The left-lateral regional shear between the Doruneh fault system and the North Kopeh Dagh fault system causes the counterclockwise rotation of the bounded blocks about vertical axis. This counterclockwise rotation of the blocks in NE Iran has been documented in many studies (e.g. Hollingsworth et al., 2010; Shabanian et al., 2009; Walker & Jackson 2004). The coeval block rotation and NE-oriented shortening leads to the formation of rhombic structures (Fig. 9). The rhombic structures are bounded on two opposite sides by thrusts (or oblique thrusts) and on the other two sides by strike-slip faults (oblique faults), which are partly overstepped. In general, the thrust and strike-slip segments bounding the rhombic structures are oblique faults and the sense of lateral-slip in adjacent sides of the rhomb is opposite (Fig. 7a & b). The faults rotate with the progressive deformation to trends oblique to the bulk shortening direction. Their rotation leads to initiation of oblique rather than pure slip along them. The degree of oblique slip depends on the degree of their rotation.

They are similar to positive flower structures in appearance and development of positive topographies but are totally different in genesis from positive flower structures developed in transpressional zones.
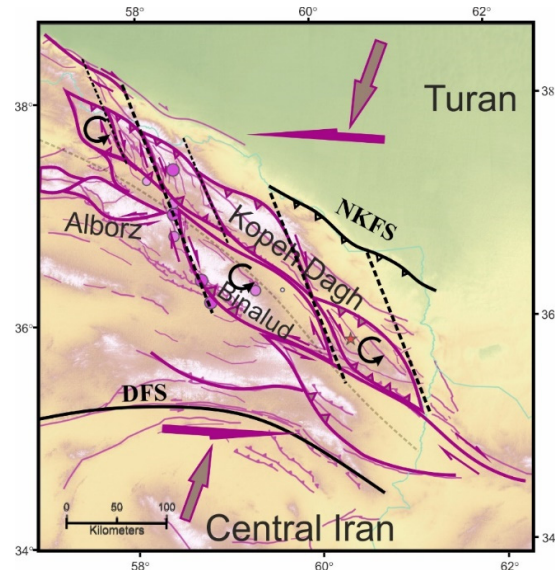
Figure 9. Simplified kinematic model of the study area plotted on the Fig. 1. This model presents formation of rhombic structures (violet rhombuses) as a result of left-lateral shear between the two deep-seated block-bounding faults, the Doruneh fault system (DFS) to the south and the North Kopeh Dagh fault system (NKFS) to the north and NE-oriented coeval shortening. Pay attention to the position of historical earthquakes (violet circles) and the recent Sefidsang earthquake (red star) concentrating at the rhombus sides. The sense of shear in adjacent sides, is opposite. The bold gray arrows present the direction of present-day compressional stress. Black dashed lines represent bounderies of counterclockwise rotating blocks. Gray dotted line shows the Atrak-Kashafrud valley which divides the Kopeh Dagh from the East Alborz-Binalud

However, there are some fundamental differences between rhombic and positive flower structures (Koyi et al., 2016):

1. The sense of movement along the bounding strike-slip faults of rhombic structures is opposite to positive flower structures. In the rhombic structure, i.e., the two sinistral strike-slip fault segments overlap in a left-step configuration, but in a positive flower structure, the strike-slip faults are in a left-step configuration, need to be dextral, not sinistral.

2. Unlike in positive flower structures, where the thrusts dip towards each other, dip direction of thrusts in the rhombic structures can vary. This is because the thrusts are the result of regional shortening, not a local shortening due to strike-slip faulting.

3. In ″regular″ flower structures, the thrusts form as a result of movement along the strike-slip faults and are active only within the area of the influence of the latter. This does not seem to be the case in rhombic structures because the thrusts are not a product of movement along the strike-slip faults, but have been formed due to regional shortening. Thrusts are not confined to the area defined by the strike-slip fault segments and seem to cut/displace the strike-slip faults that bound the same rhombic feature.

Therefore according to the following reasons, the transpressional relay zone structural model (positive flower structures) proposed by Aflaki et al. (2019) for the collision zone in NE Iran cannot be accepted. Firstly, the suggested transpressional relay zone structural model lies in a proposed larger regional system between the NW-striking main Kopeh Dagh right- lateral fault (MKDF; Shabanian et al., 2009) and the N- striking Nehbandan right- lateral fault that is more compatible with a transtensional zone than the proposed transpressional one. Secondly, the overall deformation in NE is regional shortening not a local shortening due to strike-slip faulting. In transpressional zones, the thrusts are a product of movement along the strike-slip faults. Thirdly, the existence of E-W-striking reverse and ENE-striking sinistral reverse active faults also are not explainable by their model in the region.

At last, pre-existing structures have a great impact on the pattern of neo-deformation in fold-and-thrust belts. Cimmerian-related basement faults in NE Iran confine the expansion of rhombic cells and sense of block rotation under regional shortening.

Conclusion

Earthquakes give an excellent opportunity to investigate the active deformation. In this study, April 2017 5th Mw 6.15 Sefidsang earthquake stress distribution was investigated by seismic parameters and Coulomb stress distribution. Despite its moderate kinematics magnitude, its location at the southeastern termination of the Kopeh Dagh mountains near the Cimmerian arc-related Fariman complex helps to answer some open questions on the geodynamics of northeastern Iran. Our results reveal that this earthquake occurred on a northeast-dipping listric fault with dextral reverse movement. Similar kinematics for other NW-striking and also sinistral reverse for eastwest-striking faults in the region revealed by morphotectonic data represent a typical structure known as the rhombic structure. The left-lateral regional shear between the two deep-seated block-bounding faults, the Doruneh fault system in Central Iran to the south and the North Kopeh Dagh fault system in Turan plate to the north, causes the counterclockwise rotation of the blocks about the vertical axis. The coeval block rotation and NE-shortening lead to the formation of rhombic structures in NE Iran. Recognition of the pattern and kinematics of active deformation in addition to paleo-structures can help us to shed light on structural aspects of other unknown continental block subjected to active deformation in the area. The results of this study improve our understanding about kinematics of active deformation in NE Iran and have important implications for seismic hazard assessment of the region and potential future failure area.

Aknowledgements

References

Aflaki, M., Mousavi, Z., Ghods, A., Shabanian, E., Vajedian, S., Akbarzadeh, M., 2019. The 2017 Mw 6 Sefid Sang earthquake and its implication for the geodynamics of NE Iran. Geophysical Journal International, 218(2): 1227-1245.

Aki, M., 1965. Maximum likelihood estimate of b in the formula log N = a − bM and its confidence limits. Bulletin of Earthquake Research Institute of the University of Tokyo, 43: 237-239.

Alavi, M., 1992. Thrust tectonics of the Binalood region, NE Iran. Tectonics, 11(2): 360-370.

Alavi, M., 1996. Tectonostratigraphic synthesis and structural style of the Alborz mountain system in northern Iran. Journal of Geodynamics, 21(1): 1-33.

Allen, C., Amand, P., Richter C., Nordquist J., 1965. Relation between seismicity and geological structure in the southern California region. Bulletin of the Seismological Society of America, 55: 752-797.

Ambraseys, N., Melville, C., 1982. A History of Persian Earthquakes. Cambridge University Press, Cambridge, U. K.

Aron, A., Hardebeck, J., 2009. Seismicity rate changes along the central California coast due to stress changes from the 2003 M 6.5 San Simeon and 2004 M 6.0 Parkfield earthquakes. Bulletin of the Seismological Society of America, 99: 2280-2292.

Bender, B., 1983. Maximum-likelihood estimation of b values for magnitude grouped data. Bulletin of

the Seismological Society of America, 73: 831-851.

Berberian, M., 1981. Active faulting and tectonics of Iran. In: Gupta, H. and Delany, F. (Eds), Zagros-Hindu Kush-Himalaya Geodynamic Evolution, Geodynamic Series, Chapter 3, American Geophysical Union, pp. 33-69.

Berberian, M., King, G., 1981. Towards a palaeogeography and tectonic evolution of Iran. Canadian Journal of Earth Sciences, 18: 210-265.

Berberian, M., Yeats, R., 1999. Patterns of historical earthquake rupture in the Iranian Plateau. Bulletin of the Seismological Society of America, 89: 120 - 139.

Berberian, M., Yeats, R., 2001. Contribution of archaeological data to studies of earthquake history in the Iranian Plateau. Journal of Structural Geology, 23: 563 - 584.

Bufe, C.G., 1970. Frequency-magnitude variations during the 1970 Danville earthquake swarm. Earthquake Notes, 41: 3-6.

Carey-Gailhardis, E., Mercier, J.-L., 1987. A numerical method for determining the state of stress using focal mechanism of earthquake populations: application to Tibetan teleseisms and microseismicity of southern Peru. Earth and Planetary Science Letters, 82: 165-179.

Catalli, F., Chan, C., 2012. New insights into the application of the Coulomb model in real-time. Geophysical Journal International, 188(2): 583-599.

Catalli, F., Meier, M., Wiemer, S., 2013. The role of Coulomb stress changes for injection-induced seismicity: the Basel enhanced geothermal system. Geophysical Research Letters, 40: 72-77.

Darvishzadeh, A., 1991. Geology of Iran. Neda Publication, Tehran, Iran, 901pp. (in Persian).

Das, S., Scholz, C. H., 1981. Off-fault aftershock clusters caused by shear stress increase. Bulletin of the Seismological Society of America, 71: 1669-1675.

DeMets, C., Gordon, R. G., Argus, D. F., Stein, S., 1994. Effect of recent revisions to the geomagnetic reversal timescale on estimates of current plate motions. Geophysical Research Letters, 21(20): 2191- 2194.

Deng, J., Sykes, L.R., 1997. Stress evolution in southern California and triggering of moderate, small, and micro-size earthquakes. Journal of Geophysical Research, 102: 24411-24435.

England, P., Jackson, J., 1989. Active deformation of the continents. Annual Reviews of Earth and Planetary Science, 17: 197-226.

Gibowicz, S.J., 1973. Variation of the frequency-magnitude relation during earthquake sequences in New Zealand. Bulletin of the Seismological Society of America, 63: 517-528.

Görgün, E., Zang, A., Bohnhoff, M., Milkereit, C., Dresen, G., 2009. Analysis of Izmit aftershocks 25 days before the November 12th 1999 Düzce earthquake, Turkey. Tectonophysics, 474 (3-4): 507-515.

Guest, B., Axen, G., Lam, P., Hassanzadeh, J., 2006. Late Cenozoic shortening in the west-central Alborz Mountains, northern Iran, by combined conjugate strike-slip and thin-skinned deformation, Geosphere, 2(1): 35-52.

Gutenberg, B., Richter, C.F., 1944. Frequency of earthquakes in California. Bulletin of the Seismological Society of America, 34: 185-188.

Haji Aghajany, S., Pirooznia, M., Raoofian Naeeni, M., Amerian, Y., 2020. Combination of Artificial Neural Network and Genetic Algorithm to Inverse Source Parameters of Sefid-Sang Earthquake Using InSAR Technique and Analytical Model Conjunction. Journal of the Earth and Space Physics, 45(4): 121-131.

Hainzl, S., Moradpour, J., Davidsen, J., 2014. Static stress triggering explains the empirical aftershock distance decay. Geophysical Research Letters, 41: 8818-8824.

Hainzl, S., Steacy, S., Marsan, D., Seismicity models based on Coulomb stress calculations. Community Online Resource for Statistical Seismicity Analysis (2010), http://dx.doi.org/10.5078/corssa-32035809

Hardebeck, J., Nazareth, J.J., Hauksson, E., 1998. The static stress change triggering model: constraints from two southern California aftershock sequences. Journal of Geophysical Research, 103: 24427-24437.

Harris, R., 1998. Introduction to special section: stress triggers, stress shadow, and implications for seismic hazard. Journal of Geophysical Research, 103: 24347-24358.

Harris, R., Simpson, R.W., 1998. Suppression of large earthquakes by stress shadows: a comparison of Coulomb and rate-state failure. Journal of Geophysical Research, 103: 24439-24451.

Harris, R., Simpson, R.W., Reasenberg, P.A., 1995. Influence of static stress changes on earthquake locations in southern California. Nature, 375: 221-224.

Hatzidimitriou, P., Papadimitriou Mountrakis, D., Papazachos, B., 1985. The seismic parameter b of the frequency-magnitude relation and its association with the geological zones in the area of Greece. Tectonophysics, 120: 141-151.

Hollingsworth, J., 2007. The active tectonics of NE Iran, Ph.D. thesis, University of Cambridge, Cambridge, U. K.

Hollingsworth, J., Fattahi, M., Walker, R., Talebian, M., Bahroudi, A., Bolourchi, M.J., Jackson, J., Copley, A., 2010. Oroclinal bending, distributed thrust and strike-slip faulting, and the accommodation of Arabia-Eurasia convergence in NE Iran since the Oligocene. Geophysical Journal International, 181: 1214-1246.

Ishibe, T., Shimazaki, K., Tsuruoka, H., Yamanaka, Y., Satake, K., 2011. Correlation between Coulomb stress changes imparted by large historical strike-slip earthquakes and current seismicity in Japan. Earth, Planets, Space, 63: 301- 314. http://dx.doi.org/10.5047/eps.2011.01.008.

Jackson, J., 1992. Partitioning of strike-slip and convergent motion between Eurasia and Arabia in eastern Turkey and the Caucasus. Journal of Geophysical Research, 97: 12471-12479.

Jackson, J.A., McKenzie, D.P., 1984. Active tectonics of the Alpine-Himalayan Belt between western Turkey and Pakistan. Geophysical Journal of the Royal Astronomical Society, 77: 185-264.

Karimpour, M.H., Stern, C.R., Farmer, L., 2010. Zircon U-Pb geochronology, Sr-Nd isotope analyses, and petrogenetic study of Dehnow diorite and Kuhsangi granodiorite (Paleo-tethys), NE Iran. Journal of Asian Earth Sciences, 37: 384-393.

King, G. C. P., Stein, R. S., and Lin, J., 1994. Static stress changes and triggering of earthquakes. Bulletin of the Seismological Society of America, 84: 935-953.

Koyi, H., Nilfouroushan, F. and Hessami, K., 2016. Modelling role of basement block rotation and strike-slip faulting on structural pattern in cover units of fold-and-thrust belts. Geological Magazine, 153(5-6): 827-844. doi: 0.1017/S0016756816000595

Kozłowska, M., Orlecka-Sikora, B., Kwiatek, G., Boettcher, M.S., Dresen, G., 2015. Nanoseismicity and picoseismicity rate changes from static stress triggering caused by a Mw 2.2 earthquake in Mponeng gold mine, South Africa. Journal of Geophysical Research: Solid Earth, 120: 290-307.

Lin, J., Stein, R.S., 2004. Stress triggering in thrust and subduction earthquakes, and stress interaction between the southern San Andreas and nearby thrust and strike-slip faults. Journal of Geophysical Research: Solid Earth, 109, B02303. http://dx.doi.org/10.1029/2003JB002607.

Lin, J., Stein, R.S., Meghraoui, M., Toda, S., Ayadi, A., Dorbath, C., Belabbes, S., 2011. Stress transfer among en echelon and opposing thrusts and tear faults: triggering caused by the 2003 Mw = 6.9 Zemmouri, Algeria, earthquake. Journal of Geophysical Research: Solid Earth, 116, B03305. http://dx.doi.org/10.1029/2010JB007654

Lyberis, N. and Manby, G., 1999. Oblique to orthogonal convergence across the Turan block in the post-Miocene. American Association of Petroleum Geologists Bulletin, 83(7): 1135-1160.

Ma, K.F., Chan, C.H., Stein, R.S., 2005. Response of seismicity to Coulomb stress triggers and shadows of the 1999 Mw = 7.6 Chi-Chi, Taiwan, earthquake. Journal of Geophysical Research: Solid Earth, 110, B05S19. http://dx.doi.org/10.1029/2004JB003389.

Masson, F., Anvari, M., Djamour, Y., Walpersdorf, A., Tavakoli, F., Daignières, M., Nankali, H., Van Gorp, S., 2007. Large-scale velocity field and strain tensor in Iran inferred from GPS measurements: new insight for the present-day deformation pattern within NE Iran. Geophysical Journal International, 170(1): 436-440.

McCaffrey, R., 1991. Slip vectors and stretching of the Sumatran fore arc. Geology, 19(9): 881-884.

McClusky, S., Reilinger, R., Mahmoud, S., Ben Sari, D., Tealeb, A., 2003. GPS constraints on Africa (Nubia) and Arabia plate motions. Geophysical Journal International, 155(1): 126-138.

McKenzie, D., Jackson, J., 1986. A block model of distributed deformation by faulting. Journal of the Geological Society, 143(2): 349-353.

Meier, M.-A., Werner, M.J., Woessner, J., Wiemer, S., 2014. A search for evidence of secondary static stress triggering during the 1992 Mw7.3 Landers, California, earthquake sequence. Journal of Geophysical Research: Solid Earth, 119. http://dx.doi.org/10.1002/ 2013JB010385.

Mitsakaki, C., Rondoyanni, Th., Anastasiou, D., Papazissi, K., Marinou, A., Sakellariou, M., 2013. Static stress changes and fault interactions in Lefkada Island. Western Greece. Journal of

Geodynamics, 67: 53-61.

Mogi, K., 1967. Regional variation in magnitude-frequency relation of earthquake. Bulletin of the Seismological Society of America, 45: 313-325.

Motaghi, K., Tatar, M., Shomali, Z.H., Kaviani, A., Priestley, K., 2012. High resolution image of uppermost mantle beneath NE Iran continental collision zone. Physics of the Earth and Planetary Interiors, 208-209: 38-49.

Mousavi, Z., Walpersdorf, A., Walker, R.T., Tavakoli, F., Pathier, E., Nankali, H.R.E.A., Nilfouroushan, F., Djamour, Y., 2013. Global Positioning System constraints on the active tectonics of NE Iran and the South Caspian region. Earth and Planetary Science Letters, 377: 287-298.

Naimi Ghassabian, N., Shaifi, H., Akbari Moghaddam, M., 2017. Report of earthquake MW 6.15 Sefidsang Mashhad 2017.04.05. Mashhad: Geological Survey of NE Iran, 73 pp.

Natal'in, B.A., Sengör, A.M.C., 2005. Late Palaeozoic to Triasic evolution of the Turan and Scythian platforms: the pre-history of the Palaeo-Tethyan closure. Tectonophysics, 404: 175-202.

Parsons, T., 2002. Global Omori law decay of triggered earthquakes: large aftershocks outside the classical Aftershock Zone. Journal of Geophysical Research: Solid Earth, 107. http://dx.doi.org/10.1029/2001JB000646

Parsons, T., 2005. Significance of stress transfer in time-dependent earthquake probability calculations. Journal of Geophysical Research: Solid Earth, 110. http://dx.doi.org/10.1029/2004JB003190

Parsons, T., Segou, M., Sevilgen, V., Milner, K., Field, E., Toda, S., Stein, R.S., 2014. Stress-based aftershock forecasts made within 24 h postmain shock: expected north San Francisco Bay area seismicity changes after the 2014 M = 6.0 West Napa earthquake. Geophysical Research Letters, 41: 8792-8799.

Parsons, T., Stein, R.S., Simpson, R.W., Reasenberg, P.A., 1999. Stress sensitivity of fault seismicity: a comparison between limited-offset oblique and major strike-slip faults. Journal of Geophysical Research, 104: 20183-20202.

Ruttner, A.W., 1991. Geology of the Aghdarband area (Kopet Dagh, NE-Iran). Abhandlungen der Geologischen Bundesanstalt, 38: 7-79.

Sarkarinejad, K., Ansari, S., 2014. The Coulomb stress changes and seismicity rate due to the 1990 Mw 7.3 Rudbar earthquake. Bulletin of the Seismological Society of America, 104: 2943- 2952. Doi: http://dx.doi.org/10.1785/01 20130314

Sarkarinejad, K., Ansari, S., 2015. Did the 1983 Charazeh earthquake trigger the 1990 destructive Rudbar earthquake? International Journal of Earth Sciences, 104: 309-319.

Scholz, C.H., 1968. The frequency magnitude relation of microfracturing in rock and its relation to earthquakes. Bulletin of the Seismological Society of America, 58 (1): 399-415.

Scholz, C. H., 1990. The Mechanics of Earthquakes and Faulting. Cambridge University Press, New York.

Schorlemmer, D., Wiemer, S., 2005. Microseismicity data forecasts rupture area. Nature, 434, 1086.

Schorlemmer, D., Wiemer, S., Wyss, M., 2004. Earthquake statistics at Parkfield: 1. Stationarity of b values. Journal of Geophysical Research, 109, B12307. doi: 10.1029/2004JB003234

Sengör, A.M.C., 1984. The Cimmeride orogenic system and the tectonic of Eurasia. Geological Society of America Special Papers, 195, 82 pp.

Shabanian, E., Bellier, O., Siame, L., Arnaud, N., Abbassi, M. R., Cochemé, J. J., 2009. New tectonic configuration in NE Iran: Active strike-slip faulting between the Kopeh Dagh and Binalud mountains, Tectonics, 28, TC5002. Doi: https://doi.org/10.1029/2008TC002444

Sobiesiak, M., Meyer, U., Schmidt, S., Götze, H.-J., Krawczyk, C.M., 2007. Asperity generating upper crustal sources revealed by b value and isostatic residual anomaly grids in the area of Antofagasta, Chile. Journal of Geophysical Research, 112, B12308. Doi: 10.1029/2006JB004796

Steacy, S., Gomberg, J., Cocco, M., 2005. Introduction to special section: stress transfer, earthquake triggering, and time-dependent seismic hazard. Journal of Geophysical Research, 110, B05S01. Doi: http://dx.doi.org/10.1029/ 2005JB003692.

Stein, R., 1999. The role of stress transfer in earthquake occurrence. Nature, 402: 605-609.

Stein, R.S., Barka, A.A., Dieterich, J.H., 1997. Progressive failure on the North Anatolian fault since 1939 by earthquake static stress triggering. Geophysical Journal International, 128: 594-604.

Stein, R. S., King, G. C. P., Lin, J., 1992. Change in failure stress on the southern San Andreas fault system caused by the 1992 magnitude = 7.4 Landers earthquake. Science, 258: 1328-1332

Stein, R.S., King, G.C.P., Lin, J., 1994. Stress triggering of the 1994 M = 6.7 Northridge, California earthquake by its predecessors. Science, 265: 1432-1435.

Stöcklin, J., 1974. Possible ancient continental margins in Iran. In: Burke, C. and Drake, C. (Eds.), Geology of Continental Margins. Springer-Verlag New York, pp. 873-877.

Su, Z., Yang, Y.H., Li, Y.S., Xu, X.W., Zhang, J., Zhou, X., Ren, J.J., Wang, E.C., Hu, J.C., Zhang, S.M., Talebian, M., 2018. Coseismic displacement of the 5 April 2017 Mashhad earthquake (Mw 6.1) in NE Iran through Sentinel-1A TOPS data: New implications for the strain partitioning in the southern Binalud Mountains. Journal of Asian Earth Sciences, 169: 244-256, Doi: https://doi.org/10.1016/j.jseaes.2018.08.010

Sumy, D.F., Cochran, E.S., Keranen, K.M., Wei, M., Abers, G.A., 2014. Observations of static Coulomb stress triggering of the November 2011 M5.7 Oklahoma earthquake sequence. Journal of Geophysical Research: Solid Earth, 119: 1904-1923. http://dx. doi.org/10.1002/2013JB010612.

Tchalenko, J.S., 1975. Seismicity and structure of the Kopet Dagh (Iran, USSR). Philosophical Transactions of the Royal Society of London. Series A, Mathematical and Physical Sciences, 278 (1275): 1-28.

Toda, S., 2008. Coulomb stresses imparted by the 25 March 2007 Mw =6.6 Noto-Hanto, Japan, earthquake explain its 'butterfly' distribution of aftershocks and suggest a heightened seismic hazard. Earth, Planets, Space, 60: 1041-1046.

Toda, S., Lin, J., Meghraoui, M., Stein, R.S., 2008. 12 May 2008 M = 7.9 Wenchuan, China, earthquake calculated to increase failure stress and seismicity rate on three major fault systems. Geophysical Research Letters, 35, L17305. http://dx.doi.org/10.1029/2008GL034903.

Toda, S., Stein, R.S., Sevilgen, V., Lin, J., Coulomb 3.3 graphic-rich deformation and stress-change software for earthquake, tectonic, and volcano research and teaching-user guide. U.S. Geological Survey Open-File Report 2011-1060 (2011).

Tormann, T., Wiemer, S., Hardebeck, J., 2012. Earthquake recurrence models fail when earthquakes fail to reset the stress field. Geophysical Research Letters, 39, L18310. http://dx.doi.org/10.1029/2012GL052913.

Tsapanos, T., 1990. b-value of two tectonic parts in the circum-Pacific belt, Pure and Applied Geophysics, 143: 229-242.

Urbancic, T. I., Trifu, C-I., Long, J. M., Young, R.P., 1992. Space-time correlation of b values with stress release, Pure and Applied Geophysics, 139 (3/4): 449-462.

Ustu, T., 1965. A method in determining the value of b in a formula logn =a-bM showing the magnitude frequency for earthquakes. Geophysical Bulletin of Hokkaido University, 13: 99-103.

Vernant, P., Nilforoushan, F., Hatzfeld, D., Abbassi, M.R., Vigny, C., Masson, F., Nankali, H., Martinod, J., Ashtiani, A., Bayer, R., Tavakoli, F., Chéry, J., 2004. Present-day crustal deformation and plate kinematics in the Middle East constrained by GPS measurements in Iran and northern Oman. Geophysical Journal International, 157 (1): 381-398.

Walker, R., Jackson, J., 2004. Active tectonics and late Cenozoic strain distribution in central and eastern Iran. Tectonics, 23, TC5010. doi:10.1029/2003TC001529.

Wang, J., Xu, C., Freymueller, J.T., Li, Z., Shen, W., 2014. Sensitivity of Coulomb stress change to the parameters of the Coulomb failure model: a case study using the 2008 Mw 7.9 Wenchuan earthquake. Journal of Geophysical Research: Solid Earth, 119. http://dx.doi.org/10.1002/2012JB0098 60

Wang, J.C., Shieh, C.F., Chang, T.M., 2003. Static stress changes as a triggering mechanism of a shallow earthquake: case study of the 1999 Chi-Chi (Taiwan) earthquake. Physics of the Earth and Planetary Interiors, 135: 17-25. Doi: http://dx.doi.org/10.1016/S0031-9201(02)00175-9

Wang, W.H., Chen, C.H., 2001. Static stress transferred by the 1999 Chi-Chi, Taiwan, earthquake: effects on the stability of the surrounding fault systems and aftershock triggering with a 3D fault-slip model. Bulletin of the Seismological Society of America, 91: 1041-1052.

Wells, D. L., and Coppersmith, K. J., 1994. New empirical relationships among magnitude, rupture length, rupture width, rupture area, and surface displacement. Bulletin of the Seismological Society of America, 84: 974-1002.

Wiemer, S., 2001. A Software Package to Analyze Seismicity: ZMAP. Seismological Research Letters, 92: 373-382.

Wiemer, S., Katsumata, K., 1999. Spatial variability of seismicity parameters in aftershock zones. Journal of Geophysical Research, 104 (13): 13,135-13,151.

Wiemer, S., Wyss, M., 1997. Mapping the frequency-magnitude distribution in asperities: An improved technique to calculate recurrence times? Journal of Geophysical Research, 102: 15,115-15,128.

Wiemer, S., Wyss, M., 2000. Minimum magnitude of completeness in earthquake catalogs: examples from Alaska, the Western United States, and Japan. Bulletin of the Seismological Society of America, 90: 859-869.

Wyss, M., 1973. Towards a physical understanding of the earthquake frequency distribution. Geophysical Journal of the Royal Astronomical Society, 31: 341-359.

Wyss, M., Klein, F., Nagamine, K., Wiemer, S., 2001. Anomalously high b values in the South Flank of Kilauea volcano, Hawaii: evidence for the distribution of magma below Kilauea's East rift zone. Journal of Volcanology and Geothermal Research, 106: 23-37.

Xie, C., Lei, X., Wu, X., Hu, X., 2014. Short- and long-term earthquake triggering along the strike-slip Kunlun fault, China: insights gained from the Ms 8.1 Kunlun earthquake and other modern large earthquakes. Tectonophysics, 617: 114-125.

Yadav, R.B.S., Gahalaut, V.K., Chopra, S., Shan, B., 2012. Tectonic implications and seismicity triggering during the 2008 Baluchistan, Pakistan earthquake sequence. Journal of Asian Earth Sciences, 45: 167-178.

Zanchetta, S., Berra, F., Zanchi, A., Bergomi, M., Caridroit, M., Nicora, A., Heidarzadeh, G., 2013. The record of the Late Palaeozoic active margin of the Palaeotethys in NE Iran: Constraints on the Cimmerian orogeny. Gondwana Research, 24: 1237-1266.